Journal of Power Sources 217 (2012) 13–20

Contents lists available at SciVerse ScienceDirect

Journal of Power Sources

journal homepage: www.elsevier.com/locate/jpowsour

Reversible lithium charge–discharge property of bi-capped Keggin-type polyoxovanadates

Shinya Uematsu, Zhen Quan, Yoshiaki Suganuma, Noriyuki Sonoyama*

Department of Materials Science and Engineering, Nagoya Institute of Technology, Gokiso-cyo, Showa-ku, Nagoya 466-8555, Japan

HIGHLIGHTS

- Molecular cluster ion $(KH)_9[PV_{14}O_{42}]$ was found to show charge–discharge ability.
- $(KH)_9[PV_{14}O_{42}]$ (KPV) has high discharge capacity over 200 mAh g^{-1}.
- KPV kept 95% of its initial discharge capacity after 50 cycles of charge–discharge.
- Molecular cluster ion presents stably during charge–discharge process.
- KPV reacts with lithium ion as a cluster ion molecule after 1st discharge.

ARTICLE INFO

Article history:
Received 5 March 2012
Received in revised form
21 May 2012
Accepted 28 May 2012
Available online 1 June 2012

Keywords:
Lithium intercalation
Molecular cluster ions
Bi-capped Keggin type polyoxometalates

ABSTRACT

As a new molecular cluster cathode material for lithium batteries, $K_{5.72}H_{3.28}[PV_{14}O_{42}]$ (KPV), a hetero polyoxovanadate with a bi-capped Keggin structure, was synthesized. Its crystal structure was refined by X-ray Rietveld analysis, and its electrochemical properties were examined. The symmetry space group of KPV was assigned to FM3-M. The $[PV_{14}O_{42}]^{9-}$ bi-capped Keggin units are connected sharing K^+ ions. KPV contains many cation site vacancies and has tunnels facing various directions. The polycrystalline KPV powder becomes amorphous when dried at 80 °C, while the molecular cluster structure of KPV, identified by Raman scattering method, is maintained.

KPV showed higher discharge capacity with higher discharge voltage than $K_3[PMo_{12}O_{40}]$ (KPM) with Keggin-type structure. The most improved property of KPV compared with KPM was cycle stability. KPV kept 95% of its initial discharge capacity after 50 cycles of discharge–charge, whereas KPM kept only 35%. The presence of bi-capped Keggin unit is confirmed by ex situ EXAFS measurement, even though a rapid amorphization of KPV was observed at the beginning of the discharge–charge process in ex situ X-ray diffraction (XRD) measurements. The results of ex situ EXAFS measurement and the reversible charge transfer resistance of KPV estimated from the AC-impedance measurement during the discharge–charge process also indicate that the cycle stability of KPV is attributable to the stability of the KPV cluster ion unit.

1. Introduction

Lithium batteries are a promising energy storage source for the next generation of electrical devices and vehicles. Current cathode materials for lithium batteries are metal oxides or phosphates including lithium ion in their lattices. For these materials, the capacity is mainly determined by the recoverability of the structure during the lithium (de-)intercalation. For example, the phase of Li_xMO_2 (M = Co or Ni) with a layered rock salt structure changes with the deintercalation of lithium from hexagonal to monoclinic and then back to hexagonal, but with a different structure from the initial state [1–3]. The recoverability of the initial hexagonal phase by lithium intercalation determines the useable limit of deintercalation to be $x = 0.5$ (monoclinic phase) [4]. For the case of $Li_xMn_2O_4$ with a spinel structure, its phase changes from cubic to tetragonal during the intercalation process in the region $x \geq 1.0$ (3 V region), accompanied by a 6% increase in the volume owing to the Jahn–Teller effect of the Mn^{3+} ion [5,6]. This volume change degrades its cycle stability and only the 4 V region of $LiMn_2O_4$ is used in commercial batteries.

Recently, cluster materials have drawn attention as a new cathode material for lithium batteries [7,8]. In a previous paper [7], we indicated that cluster ion electrodes are expected to show intermediate properties between lithium intercalation electrodes

* Corresponding author. Tel./fax: +81 52 735 7243.
E-mail address: sonoyama@nitech.ac.jp (N. Sonoyama).

0378-7753/$ – see front matter © 2012 Elsevier B.V. All rights reserved.
http://dx.doi.org/10.1016/j.jpowsour.2012.05.096

and organic radical electrodes [9–12]. Usual cluster ions consist of several (or ten-odd) metal ions in a unit. They behave as a single molecule under dissolved conditions in solvents. During the solidification process, cluster ions form ionic crystals with some counter ions, while some of them become amorphous. These cluster ion materials are expected to show redox activity as a molecular cluster, not as a continuum. Therefore, the capacity and stability of the cluster material are independent from the stability or recoverability of its crystal. Some of the clusters can be divided into metal complexes [8]. Generally, the metal complexes that contain organic ligands lack durability during the discharge–charge process [8,13,14].

We focused on the polyoxometalates, which are molecular cluster ions that consist of transition metals, oxygen, and hetero ions (P, Si, As, etc.). In a previous paper [7], we reported the electrochemical properties of Keggin-type polyoxomolybdate $K_3[PMo_{12}O_{40}]$ (KPM) as a cathode electrode for lithium batteries. KPM showed discharge–charge performance in the potential region from 4.2 V to 1.5 V with a capacity of over 200 mAh g^{-1}; however, the main discharge voltage (2.5–1.5 V) was lower than the usual lithium battery cathode materials, and its cycle stability was low. The low discharge voltage seemed to be related to the low redox potential of molybdenum, the oxide that has been studied as an anode electrode material for lithium batteries [15–17]. The composition of Keggin-type hetero polyoxometalates can be written as $[XM_{12}O_{40}]^{y-}$. The *X* ions are hetero ions, such as P or Si, and the *M* ions are addenda ions such as Mo, W, Cr, Nb, and V. For hetero polyoxometalates, vanadium is an attractive addenda ion because of its high redox potential (0.3 V higher than molybdenum ion), low molecular weight, low toxicity, and lower cost. In the present study, we focused on $K_{9-y}H_y[PV_{14}O_{42}]$ (KPV) with a bi-capped Keggin-type structure. In Fig. 1, structures of (a) Keggin-type polyoxometalate and (b) bi-capped Keggin type one were shown. As for usual Keggin type structure, twelve MO_6 octahedrons are connected with top- or side-sharing around the tetrahedral hetero ion (*X*) oxide. Alternatively, Keggin-type polyoxometalates can be regarded as four $[M_3O_9]$ units are coordinating to the XO_4 ion. For bi-capped Keggin-type polyoxometalates, two vanadyl ions (VO^{3+}) are coordinated with the Keggin-type structure to compensate for large minus charge of the cluster ion [18,19]. In this study, the crystal structure of the synthesized KPV was first refined. Measurement of electrochemical properties and ex situ XRD measurement during the discharge or charge process were carried out and compared with those of KPM to investigate the discharge–charge mechanism.

2. Experimental

Synthesis of $K_3[PMo_{12}O_{40}]$ was carried out using standard methods [20–22] and identification and annealing conditions that have been reported elsewhere [7]. $H_9[PV_{14}O_{42}]$ was synthesized using established methods [23]. Sodium ortho-vanadate ($NaVO_3$: Kishida, GR) and disodium hydrogen phosphate (Kishida, GR) with molar ratio of 1:2 were dissolved in hot water. The pH of the solution was adjusted to 2.2 by adding sulfuric acid (Kishida, GR) at 60 °C. Counter ion exchange for the specified substance was carried out by adding KCl powder (Wako, GR) to this solution. Obtained samples were dried at 80 °C for 12 h under air, unless otherwise mentioned. The composition of KPV was determined using ICP–OES (Shimadzu ICPE-9000). Identification of products was carried out by ^{51}V NMR (Varian GEMINI-300) with vanadium chloride (Strem Chemicals, GR) in distilled water as a standard, FT–IR (Jasco FT/IR-410), and Raman scattering (Jasco NRS-3300) measurements. For FT–IR measurements, a pellet with a 5ϕ

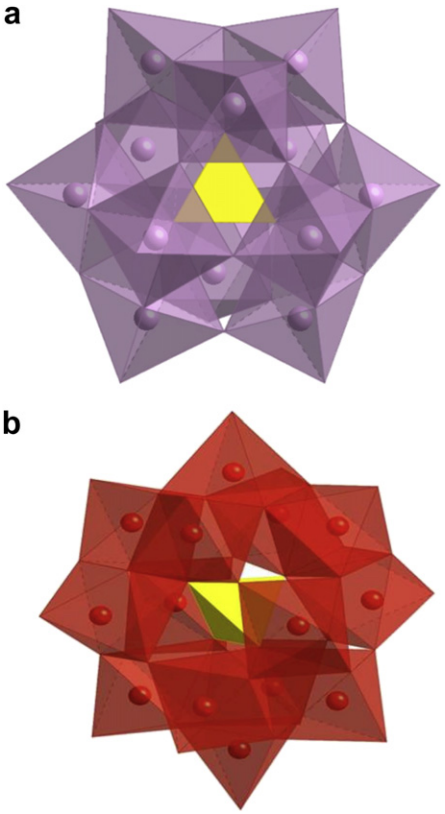

Fig. 1. Structure of (a) Keggin-type and (b) bi-capped Keggin-type polyoxometalate.

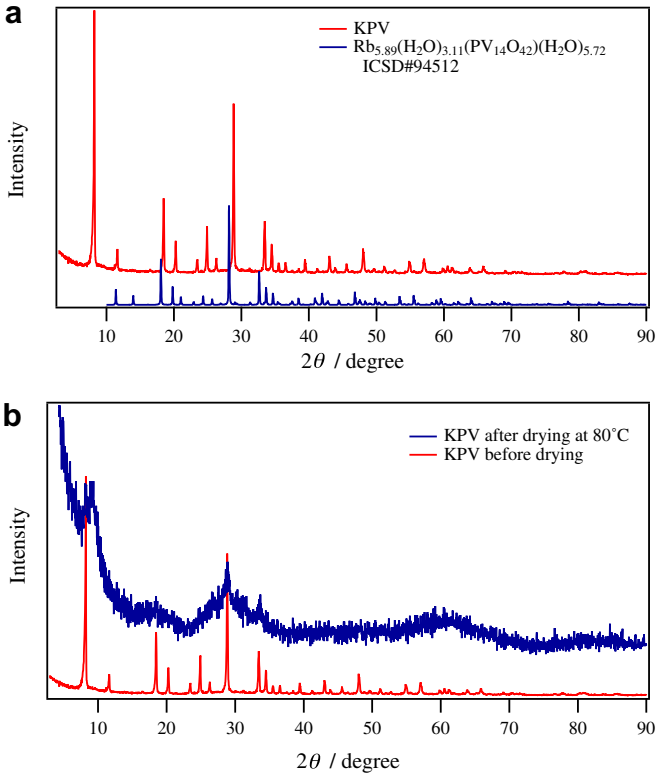

Fig. 2. XRD patterns for $K_{5.72}H_{3.28}[PV_{14}O_{42}]$ (KPV) (a) as prepared and (b) after drying process at 80 °C.

diameter was used, which was prepared from KPV and KBr mixed powder. For the probe light of Raman scattering measurements, DPSS laser with a wavelength of 532 nm was used. XRD measurements were carried out using a powder X-ray diffractometer (Rigaku RAD-C) with Cu Kα radiation. The structural parameters of samples were refined by the Rietveld analysis [24] using the computer program RIETAN-2000 [25]. The electrochemical performance of cells was studied by discharge–charge cycle tests and AC-impedance measurements at 25 °C. The cathode consisted of 30 wt% active material, 65 wt% acetylene black, and 5 wt% PTFE binder. Ethylene carbonate–diethyl carbonate mixed solvent (7:3) with a supporting electrolyte of 1 M $LiPF_6$ (Kishida battery grade) and lithium metal (Honjyo Metal) were used as the electrolyte and anode material, respectively. The discharge–charge characteristics of the samples were examined using a CR-2032 coin cell with a battery tester (Interface model 0Z0-A19). After the discharge to various voltages and one cycle of the discharge–charge process, an ex situ XRD measurement was carried out under Ar atmosphere. For the measurement of the ex situ XRD, as prepared KPV was used without drying process.

AC-impedance spectra for cells were obtained using a frequency-response analyzer (Solatron 1255) connected with a potentiostat (Solatron 1280) in the frequency range of 10^{-2} to 10^{6} Hz with an applied potential of 0.02 V from the cell voltage.

Vanadium *K*-edge X-ray absorption spectra were recorded at beam line 7C at the Institute of Materials Structure Science (Photon Factory; ring energy of 2.5 GeV and ring current of 400–250 mA) with a conventional transmission mode. A Si(111) crystal monochromator was employed and detuned by 80% to suppress higher-order harmonics. The incident and transmitted X-ray intensities were measured by ionization chambers filled with pure N_2 30% Ne 70% mixed gas. Standard samples such as vanadium oxides and KPV

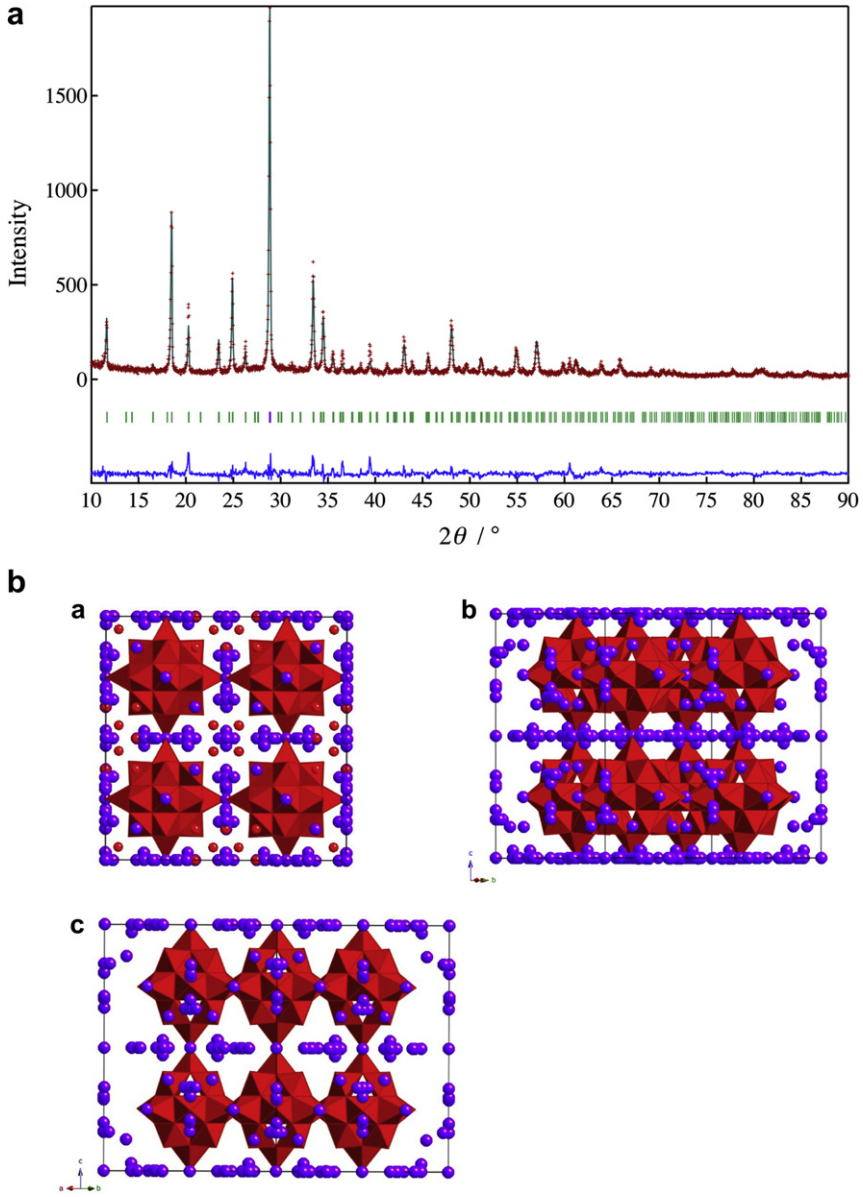

Fig. 3. (a) Rietveld refinement patterns of $K_{5.72}H_{3.28}[PV_{14}O_{42}]$ for the XRD data taken at room temperature. The observed intensity data are shown by dots, and the solid line overlying them refers to the calculated intensity. Vertical markers below the diffraction patterns indicate positions of possible Bragg reflections. Differences between the observed and calculated intensities are plotted at the bottom, in the same scale. (b) Crystal structure of $K_{5.72}H_{3.28}[PV_{14}O_{42}]$ refined by Rietveld analysis in the (a) (100), (b) (1–10) and (c) (110) planes with the V^{5+}-centered polyhedron.

dried at 80 °C were diluted with acetylene black and formed into the pellets for the measurements. For the cycled samples, cathode materials were removed from the separable cells (Hosen HS cell) in the helium atmosphere glove box and set into the sealed aluminum cell equipped with Mylar film windows.

3. Results and discussion

The ^{51}V NMR spectrum for KPV, which was synthesized in the present study and dissolved in distilled water, was measured. Three main peaks were observed, and the positions of these peaks were in agreement with those reported by Domaille [26]. The FT–IR spectrum of KPV in the KBr disk was also measured for the identification. The absorption at 1050 cm^{-1} is assigned to P–O stretching vibration, and the lower wave numbers are assigned to V–O stretching vibration. The position of these peaks also agreed with those in previous reports [23,27]. The composition of the KPV was determined by inductively coupled plasma optical emission spectrometry (ICP–OES) to be $K_{5.72}H_{3.28}[PV_{14}O_{42}]$.

The XRD pattern for KPV without drying is shown in Fig. 2(a). The XRD pattern for KPV was similar to that of $Rb_{5.89}(H_3O)_{3.11}(PV_{14}O_{42})(H_2O)_{5.72}$ [28], although the XRD pattern and crystal structure of KPV have not been reported, to the best of our knowledge. The crystal structure of KPV was refined by Rietveld analysis on the basis of the structure of $Rb_{5.89}(H_3O)_{3.11}(PV_{14}O_{42})(H_2O)_{5.72}$, of which the symmetry space group was assigned to FM3-M. The result of the refinement is shown in Fig. 3(a), and the obtained parameters from the structure refinement are summarized in Table 1. The crystal structure of KPV on the basis of the Rietveld refinement is shown in Fig. 3(b). The $[PV_{14}O_{42}]^{9-}$ bi-capped Keggin units are connected sharing K^+ ions. There are many cation sites other than the K^+ ion site shared by $[PV_{14}O_{42}]^{9-}$ units. Because the occupancies of these sites are low (0.01–0.25), KPV contains many vacancies, and the structure of crystallized KPV also has tunnels toward various directions. It is clear that KPV has many spaces in its crystal, and its structure is stabilized by crystal water. In Fig. 2(b), the XRD pattern for KPV dried at 80 °C is shown. All of the main reflections for KPV disappeared. This meant that the crystal of KPV became amorphous by removing the crystal water. Some polyoxometalates are known to be difficult to crystallize without containing a certain amount of crystal water. KPV seems to be one of these, and KPV powder easily became amorphous in the drying process.

In Fig. 4(a), the discharge–charge curves for KPV obtained in the voltage range from 4.2 to 1.5 V are shown along with the curves for KPM for comparison. In the discharge process, a plateau appeared at 3.5–2.5 V, and maximum discharge capacity was obtained in the third cycle (about 230 mAh g^{-1}). The discharge–charge curves for KPV without drying are shown in Fig. 4(b) and were almost the same as those of the dried KPV sample. In Fig. 5, the Raman

Table 1
Rietveld refinement results for $K_{5.72}H_{3.28}[PV_{14}O_{42}]$.

Atom	Site	g	x	y	z
K(1)	4a	0.0581	0.0	0.0	0.0
K(2)	24e	0.0177	0.0	0.0	0.16127
K(3)	24e	0.0165	0.0	0.0	0.159505
K(4)	24e	0.0289	0.0	0.0	0.159636
K(5)	96j	0.0212	0.0	−7.94E−06	0.159689
K(6)	24e	0.0967	0.0	0.0	0.191797
K(7)	24e	0.0781	0.0	0.0	0.192998
K(8)	24e	0.0633	0.0	0.0	0.194297
K(9)	24e	0.0511	0.0	0.0	0.159932
K(10)	24e	0.2323	0.0	0.0	0.302745
K(11)	24e	0.2402	0.0	0.0	0.341469
K(12)	24e	0.1271	0.0	0.0	0.289075
K(13)	24e	0.0329	0.0	0.0	0.341128
K(14)	24e	0.0288	0.0	0.0	0.193746
K(15)	24e	0.0104	0.0	0.0	0.193646
K(16)	4b	0.2401	0.0	0.0	0.5
K(17)	48h	0.010	0.0	0.249995	0.249995
K(18)	96k	0.017	−5.77E−06	−5.77E−06	0.710344
K(19)	48i	0.01	0.0	0.250002	0.249998
K(20)	48h	0.27	0.0	0.127418	0.127418
K(21)	24d	0.16	0.25	0.25	0.0
V(1)	96k	1.0	0.134469	0.244953	0.134469
V(2)	48g	0.333	0.25	0.25	5.57E−02
P	8c	1.0	0.25	0.25	0.25
O(1)	32f	1.0	0.210982	0.289018	0.210982
O(2)	96k	1.0	0.196052	0.196052	1.01E−01
O(3)	96k	1.0	9.49E−02	0.252525	9.49E−02
O(4)	96k	1.0	0.191458	0.308542	0.105473
O(5)	96j	0.1667	0.250001	0.250008	0.0
O(6)	48i	1.0	0.0	0.127037	0.372963
O(7)	48h	0.276	0.0	0.25	0.25
O(8)	32f	0.180	4.82E−02	4.82E−02	4.82E−02

Space group Fm3-m, $a = 21.3964$ Å, $R_{wp} = 18.22$, $R_p = 13.73$, $R_R = 27.98$, $R_e = 12.98$, $S = 1.40$.

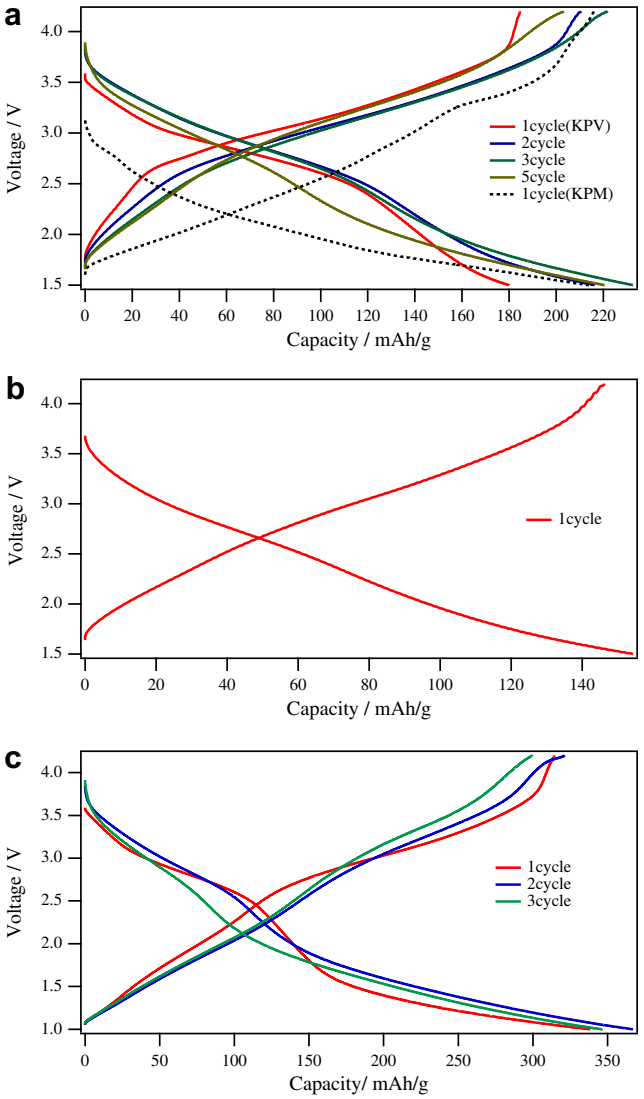

Fig. 4. Discharge–charge curves for (a) $K_{5.72}H_{3.28}[PV_{14}O_{42}]$ (KPV) after 80 °C drying/EC-DEC $LiPF_6$/Li cell in the voltage range 4.2–1.5 V; (b) KPV without drying process/EC-DEC $LiPF_6$/Li cell in the voltage range 4.2–1.5 V; (c) KPV without drying/EC-DEC $LiPF_6$/Li cell in the voltage range 4.2–1.0 V. For all the systems, current was set at 100 μA.

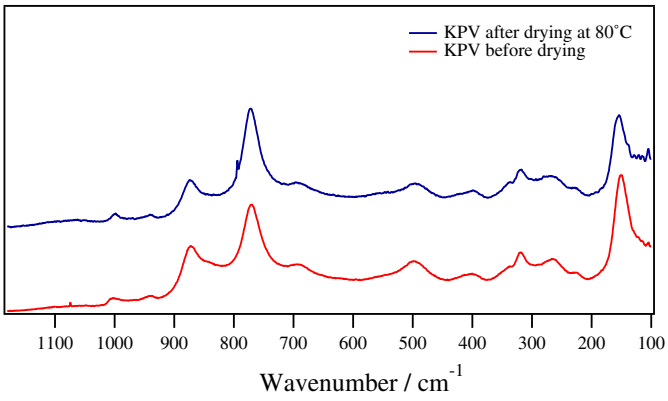

Fig. 5. Raman scattering spectra for $K_{5.72}H_{3.28}[PV_{14}O_{42}]$ (KPV) before and after the 80 °C drying process.

scattering spectra of KPV before and after the drying process are shown. Although the Raman spectrum of KPV is complicated, and it is not easy to assign bands, the Raman spectrum of KPV showed no change by drying. These results indicated that the structure of the KPV cluster ion unit was maintained after the amorphization of its crystal, and amorphization did not influence the electrochemical properties of KPV.

As can be seen in Fig. 4(a), the discharge voltage obviously is higher than that of KPM: the average discharge voltage was about 2.7 V for KPV, whereas that of KPM was 2.1 V. This increase in voltage was larger than the difference in the redox potential between V^{5+} and Mo^{6+}. The higher ionicity of $[PV_{14}O_{42}]^{9-}$, induced by its high formal charge, raised the redox potential of KPV. In Fig. 4(c), discharge–charge curves in the voltage range 4.2–1.0 V are shown. KPV showed reversible discharge–charge capability with an initial capacity of 370 mAh g^{-1}. These results suggested that multi-step reduction of vanadium (from 5+ to 3+) was proceeding during the discharge process because the ideal capacity for KPV in the single step reduction was estimated to be 212.3 mAh g^{-1}.

The relationships between the cycle number and the discharge capacity for KPM and KPV are shown in Fig. 6. From the initial capacity, 95% was kept for KPV, whereas only 37.5% was kept for KPM. Such a high cycle stability for KPV has not been reported in other studies of metal complexes or cluster ion electrode materials [8,14,29].

To investigate the reason for the difference in cycle capability between KPV and KPM, an ex situ XRD measurement of KPV was carried out. For KPM, we already reported the reversible lattice expansion and contraction during lithium (de-)intercalation [7]. The main reflection of KPM shifted to a lower angle by discharge and shifted back to a higher angle by charging; however, the position of reflection did not return to the initial angle. This XRD data and low cycle stability of KPM suggested the occurrence of some structural change in the polyoxometalate cluster ion unit. Fig. 7 shows the ex situ XRD pattern of KPM after 5 cycles. The reflection intensity of KPM decreased and reflections of the impurity phase came to be observed. This result indicated that KPM was decomposing during the discharge–charge cycles.

An ex situ XRD measurement of KPV was also attempted. For the ex situ XRD measurement, a KPV sample without heating was used because KPV powder easily becomes amorphous by heating. The XRD patterns for KPV, which was discharged to various voltages, are shown in Fig. 8. KPV started to become amorphous at 2.8 V and became completely amorphous at 2.4 V. After one discharge–charge cycle, the KPV crystal was still amorphous. No reflection was observed during the discharge–charge process of KPV. From the results of the ex situ XRD measurement, the stability of the bi-capped Keggin type $[PV_{14}O_{42}]^{9-}$ cluster ion unit could not be confirmed, even though the cycle stability of KPV is much higher than that of KPM.

Therefore, for confirmation of the stability of bicapped Keggin type cluster ion unit, ex situ XAFS measurements were carried out. XAFS is an appropriate method for the investigation of the local structure of materials.

Vanadium edge XAFS measurement and analyses were performed in order to reveal structural changes of KPV during the discharge–charge process. EXAFS functions of $k^3\chi(k)$ (where k is the photoelectron wave number) were obtained by the standard procedures of preedge baseline subtraction, edge-energy determination, postedge background subtraction and normalization using the atomic absorption coefficients. Fourier transforms of the $k^3\chi(k)$ functions (the k range is around 2.5–11.0 Å^{-1}) of KPV (as prepared, after first discharge–charge cycle and after 10 cycles) are given in Fig. 9(a). KPV shows many peaks and these peaks can be roughly divided to the inside of cluster ion (~3.5 Å) and outside. The peaks at 1.2, 1.7, 2.5 Å, would be assignable to the V–O and the peaks at 2.8 and 3.3 Å to the V–V. After the 1st cycle, the profile of Fourier transform spectrum inside of the cluster ion (~3.5 Å) hardly changed except for the intensity decrease of the peak at 2.8 Å, whereas the profile of outside region (over 3.5 Å) changed. This peak at 2.8 Å would be sum of the interactions between the vanadiums at the cap position in the cluster ions and the interaction between the vanadium at the cap position and nearest vanadium in the cluster ion unit. In the result of Rietveld refinement listed in Table 1, the distance between the vanadiums at the cap position is estimated to be about 2.4 Å. However, any clear peak

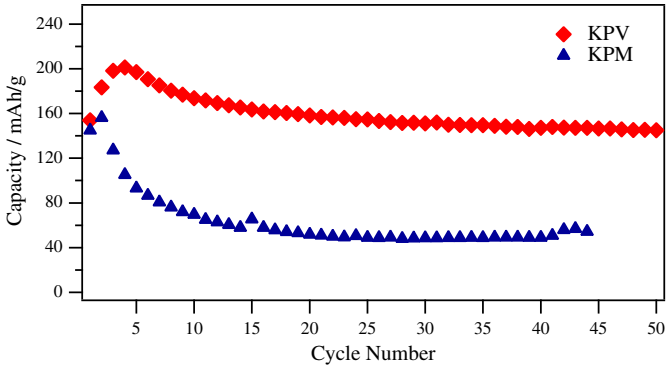

Fig. 6. Relationship between discharge capacity of $K_{5.72}H_{3.28}[PV_{14}O_{42}]$ (KPV), $K_3PMo_{12}O_{40}$ (KPM)/EC-DEC $LiPF_6$/Li cell in the voltage range 4.2–1.5 V, and the cycle numbers at a current of 100 μA.

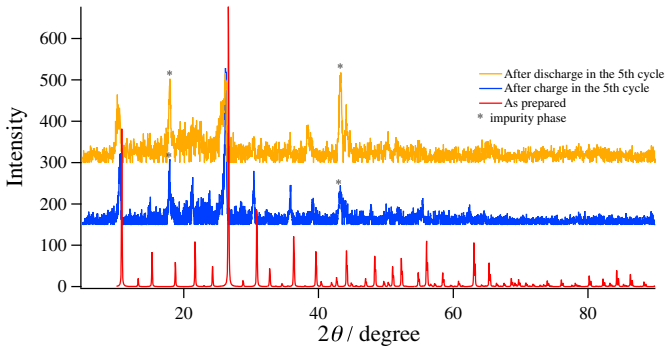

Fig. 7. Ex situ XRD patterns of $K_3PMo_{12}O_{40}$ after discharging and charging process in the 5th cycle.

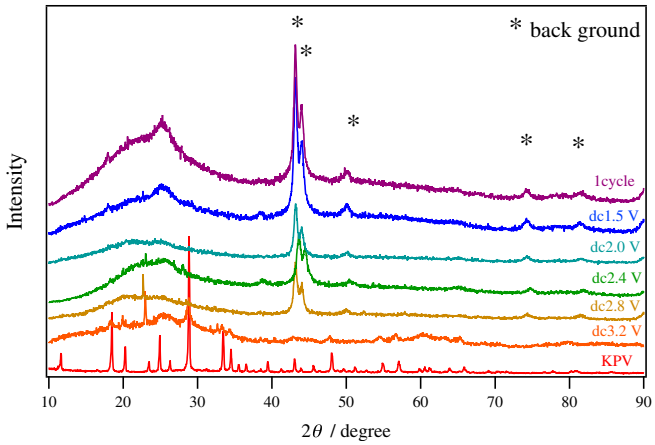

Fig. 8. Ex situ XRD patterns of $K_{5.72}H_{3.28}[PV_{14}O_{42}]$ (KPV) as prepared, after discharge to 3.2, 2.8, 2.4, 2.0, 1.5 V vs. Li, and after 1 cycle discharge–charge.

cannot be observed in Fourier transform spectrum at 2.4 Å before discharge shown in Fig. 9(a). This shift of cap position would be caused by the crystal structure change caused by the crystal water removal in the drying process.

The results shown above suggest that the molecular $[PV_{14}O_{42}]^{9-}$ ion is formed by the dismiss of the regularity in the crystal during the discharge–charge process for the following reasons. 1. The separation of crystal to the molecular ion state causes the decrease in the interaction between the vanadiums at the cap position (2.8 Å) (Fig. 2(b)). 2. The profile of Fourier transform spectrum has hardly changed in the region of cluster ion inside, whereas that in the cluster ion outside region changed after the discharge–charge process.

After 10 cycles (Fig. 9 (a)), the profile of Fourier transform spectrum inside of the cluster ion was almost the same the profile after 1st cycle. A weak peak appeared at 2.2 Å. This peak may be caused by the potassium counter ion coordinated at the surface of $[PV_{14}O_{42}]^{9-}$ ion. These results demonstrate that $[PV_{14}O_{42}]^{9-}$ ion is stable during the discharge–charge process and it is present as a cluster ion molecule at the amorphous state that appears during the discharge–charge process.

To investigate the influence of this crystal structure change on the cell reaction, AC impedance spectroscopy measurements were carried out during the discharge–charge procedure. In Fig. 10(a), Nyquist plots of KPM/EC-DEC with $LiPF_6$/Li cell in the frequency range of 10^{-2} to 10^{6} Hz at various potentials in the discharge process are shown. For the measurement of wider voltage range, AC-impedance measurement was carried out in first charge and second discharge process after discharging the cell to 1.5 V. One semicircle was found, and the radius of the circle changed with the voltage imposed on the electrode. Assuming that this semicircle was due to charge-transfer resistance, the obtained impedance

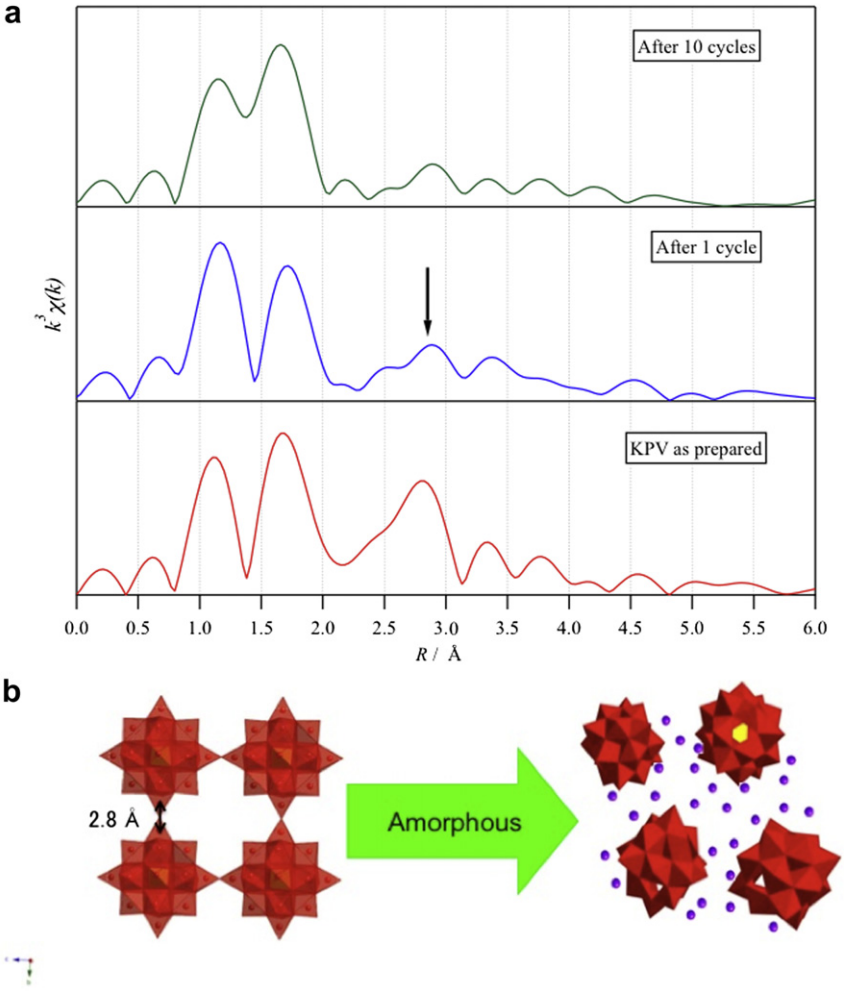

Fig. 9. (a) Fourier transforms of the $k^3\chi(k)$ functions (the k range is around 2.5–11.0 $Å^{-1}$) of ex situ EXAFS measurements for $K_{5.72}H_{3.28}[PV_{14}O_{42}]$ (as prepared, after first discharge–change cycle and after 10 cycles). (b) The image of the structural change of KPV during the first discharge–charge process.

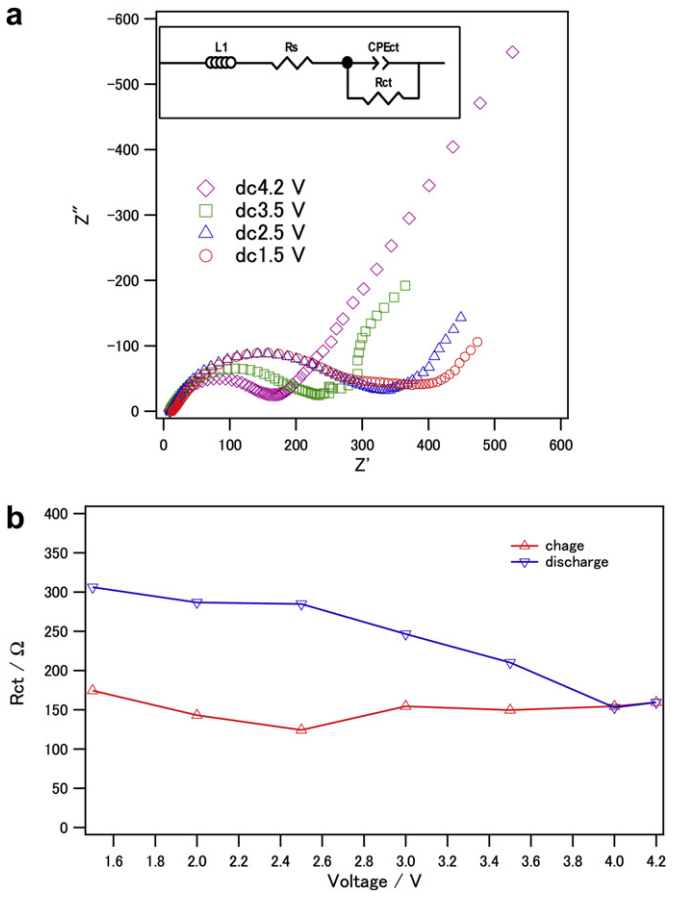

Fig. 10. (a) Nyquist plots for $K_3PMo_{12}O_{40}$/EC-DEC $LiPF_6$/Li cell at the various imposed voltages. Inset: equivalent circuit model for the cell. (b) The plot of charge transfer resistance of $K_3PMo_{12}O_{40}$/EC-DEC $LiPF_6$/Li cell as a function of the cell voltage in the first charge and second discharge process after first discharge process.

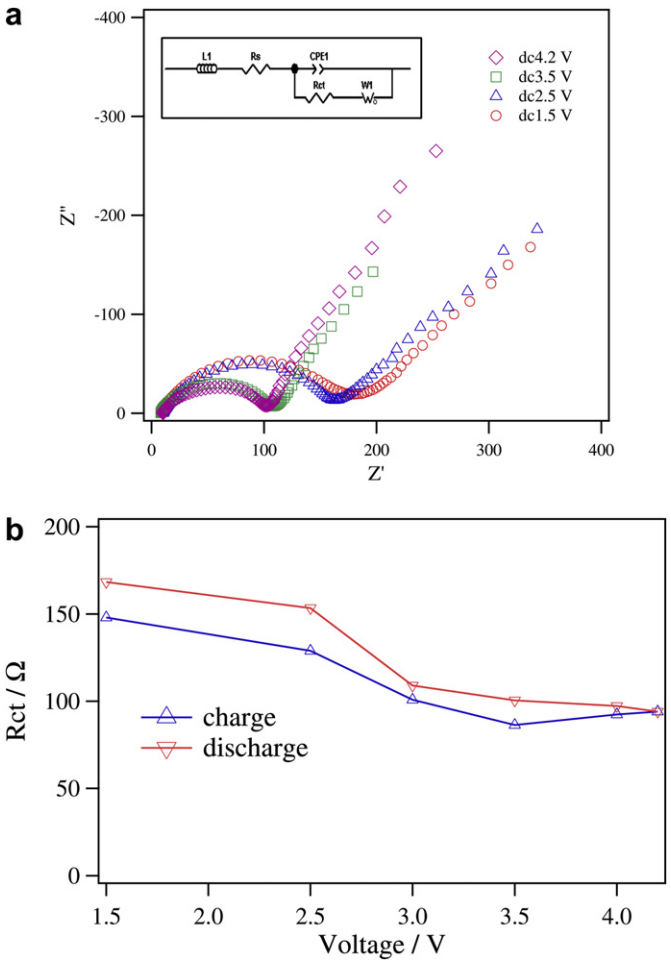

Fig. 11. (a) Nyquist plots for $K_{5.72}H_{3.28}[PV_{14}O_{42}]$/EC-DEC $LiPF_6$/Li cell at the various imposed voltages. Inset: equivalent circuit model for the cell. (b) The plot of charge transfer resistance of $K_{5.72}H_{3.28}[PV_{14}O_{42}]$/EC-DEC $LiPF_6$/Li cell as a function of the cell voltage in the first charge and second discharge process after first discharge process.

spectra were analyzed using the equivalent circuit shown in the inset of Fig. 10(a). The relationship between the charge-transfer resistance R_{ct} estimated from the Nyquist plots and the imposed voltage on the KPM is plotted in Fig. 10(b). Estimated R_{ct} increased with an imposed voltage increase during the charge process, though R_{ct} still continued increasing with the increase in voltage during the discharge process. This irreversible behavior of electrochemical properties in R_{ct} (Fig. 10(b)), the discharge–charge cycle stability (Fig. 6), and the XRD pattern change of KPM during the discharge–charge process (Fig. 7) suggest that the $[PMo_{12}O_{40}]^{3-}$ unit is damaged by discharge–charge cycles. It is known that deep reduction of $[PMo_{12}O_{40}]^{3-}$ dissolved in the solvent causes α to β isomerization of the $[PMo_{12}O_{40}]^{3-}$ ion [30] with one of the $[Mo_3O_9]$ in $[PMo_{12}O_{40}]^{3-}$ rotating 60°. Although it is not clear that this isomerization of $[PMo_{12}O_{40}]^{3-}$ occurs in the solid crystal, this structural instability of the $[PMo_{12}O_{40}]^{3-}$ unit under highly reductive conditions seems to be the reason for the low cycle stability of KPM as a lithium battery cathode material.

Nyquist plots of KPV/EC-DEC with $LiPF_6$/Li cell at various potentials in the discharge process are shown in Fig. 11(a). One small semicircle was found, and its radius became larger when decreasing the voltage imposed on the electrode. Assuming this semi-circle was due to charge-transfer resistance, the obtained impedance spectra were analyzed using the equivalent circuit shown in the inset of Fig. 11(a). The relationship between the charge-transfer resistance R_{ct} estimated from the Nyquist plots and the cell voltage on the KPV was plotted, as shown in Fig. 11(b). In the charge process, R_{ct} decreased gradually when increasing the potential and the maximum was at 1.5 V. In the discharging process, R_{ct} showed reversible dependence on the voltage. In the AC impedance measurement, a steep increase in the resistance of the cell was not found during the discharge–charge process after the amorphization of KPV. This result also suggests that the rapid amorphization during the discharge–charge process could be caused by the release of crystal water like an amorphization by drying process, not by cluster ion unit isomerization or decomposition like KPM. In other words, the $[PV_{14}O_{42}]^{9-}$ cluster ion unit is stable even after the amorphization process of KPV crystal as was confirmed by EXAFS measurement (Fig. 9). This stability of the cluster ion unit would explain the high cycle stability of KPV.

4. Conclusions

KPV showed higher energy density and cycle stability than KPM (which had an initial capacity of over 200 mAh g^{-1}). The higher cycle stability of KPV seems to be due to the structural stability of its cluster ion unit, whereas $[PMo_{12}O_{40}]^{3-}$ is decomposed by isomerization with deep discharging. The data in the present study seem to demonstrate that the stability of the molecular cluster ion cathode material is mainly dependent on the stability of the cluster ion unit, not on the recoverability of its crystal structure.

Acknowledgments

This work was financially supported by a NEDO (New Energy and Industrial Technology Development Organization) Li–EAD project.

References

[1] T. Ohzuku, A. Ueda, M. Nagayama, J. Electrochem. Soc. 140 (1993) 1862–1870.
[2] W. Li, J.N. Reimers, J.R. Dahn, Solid State Ionics 67 (1993) 123–130.
[3] G.G. Amatucci, J.M. Tarascon, L.C. Klein, J. Electrochem. Soc. 143 (1996) 1114–1123.
[4] T. Ohzuku, A. Ueda, M. Nagayama, Y. Iwakoshi, H. Komori, Electrochim. Acta 38 (1993) 1159–1167.
[5] T. Ohzuku, M. Kitagawa, T. Hirai, J. Electrochem. Soc. 137 (1990) 769–775.
[6] A. Yamada, M. Tanaka, K. Tanaka, K. Sekai, J. Power Sources 81–82 (1999) 73–78.
[7] N. Sonoyama, Y. Suganuma, T. Kume, Q. Zhen, J. Power Sources 196 (2011) 6822–6827.
[8] H. Yoshikawa, C. Kazama, K. Awaga, M. Satoh, J. Wada, Chem. Commun. (2007) 3169–3170.
[9] H. Nishide, K. Oyaizu, Science 319 (2008) 737–738.
[10] S.A. Miller, C.R. Martin, J. Am. Chem. Soc. 126 (2004) 6226–6227.
[11] J.M. Cooper, R. Cubitt, R.M. Dalgliesh, N. Gadegaard, A. Glidle, A.R. Hillman, R.J. Mortimer, K.S. Ryder, E.L. Smith, J. Am. Chem. Soc. 126 (2004) 15362–15363.
[12] K. Oyaizu, Y. Ando, H. Konishi, H. Nishide, J. Am. Chem. Soc. 130 (2008) 14459–14461.
[13] J. Yamaki, A. Yamaji, J. Electrochem. Soc. 129 (1982) 5–9.
[14] S. Okada, J. Yamaki, T. Okada, J. Electrochem. Soc. 136 (1989) 340–344.
[15] N. Kumagai, N. Kumagai, K. Tanno, Electrochim. Acta 32 (1987) 1521–1526.
[16] F. Leroux, L.F. Nazar, Solid State Ionics 133 (2000) 37–50.
[17] S. Komaba, N. Kumagai, R. Kumagai, N. Kumagai, H. Yashiro, Solid State Ionics 152–153 (2002) 319–326.
[18] R. Kato, A. Kobayashi, Y. Sasaki, J. Am. Chem. Soc. 102 (1980) 6571–6572.
[19] R. Kato, A. Kobayashi, Y. Sasaki, Inorg. Chem. 21 (1982) 240–246.
[20] G.A. Tsigdinos, Ind. Eng. Chem. Prod. Res. Dev. 13 (1974) 267–274.
[21] T.V. Andrushkevich, V.M. Bondareva, G.Y. Popova, Y.D. Pankratiev, React. Kinet. Catal. Lett. 52 (1994) 73–80.
[22] G.Y. Popova, T.V. Andrushkevich, V.M. Bondareva, I.I. Zakharov, Kinet. Katal. 35 (1994) 91–95.
[23] K. Nomiya, K. Kato, M. Miwa, Polyhedron 5 (1986) 811–813.
[24] F. Izumi, The Rietverd Method, Oxford University Press, 1993.
[25] F. Izumi, T. Ikeda, Mater. Sci. Forum 198 (2000) 321–324.
[26] P.J. Domaille, J. Am. Chem. Soc. 106 (1984) 7677–7687.
[27] E.J. Baran, C.I. Cabello, J. Mol. Struct. 174 (1988) 401–406.
[28] E.V. Murashova, A.B. Iluikhin, N.N. Chudinova, Zh. Neorg. Khim. 46 (2001) 1431–1434.
[29] N. Imanishi, T. Morikawa, J. Kondo, Y. Takeda, O. Yamamoto, N. Kinugasa, T. Yamagishi, J. Power Sources 79 (1999) 215–219.
[30] S. Himeno, T. Osakai, A. Saito, Bull. Chem. Soc. Jpn. 62 (1989) 1335–1337.